Micrometer-scale electrical breakdown in high-density fluids with large density fluctuations: Numerical model and experimental assessment

Hitoshi Muneoka,[1,2,*] Keiichiro Urabe,[1,2] Sven Stauss,[1] and Kazuo Terashima[1,†]
[1]*Department of Advanced Materials Science, Graduate School of Frontier Sciences, The University of Tokyo, Kashiwa, Chiba 277-8561, Japan*
[2]*Japan Society for the Promotion of Science, Tokyo 102-0083, Japan*
(Received 30 December 2014; published 29 April 2015)

Experimentally observed electrical breakdown voltages (U_B) in high-pressure gases and supercritical fluids deviate from classical theories for low-pressure gas discharges, and the underlying breakdown mechanisms for the high-density fluids making the U_B differ from those in the classical discharges are not yet well understood. In this study, we developed an electrical breakdown model for the high-density fluids taking into account the effects of density fluctuations and ion-enhanced field emission (IEFE). The model is based on the concept that a critical anomaly of the U_B (local minimum near the critical point) is caused by long mean free electron path leading to a large first Townsend coefficient in locally low-density spatial domains generated by the density fluctuations. Also, a modified Paschen's curve considering the effect of the IEFE on the second Townsend coefficient was used to reproduce the U_B curve in the high-density fluids. Calculations based on the novel model showed good agreements with the experimentally measured U_B even near the critical point and it also suggested that the critical anomaly of the U_B depends on the gap distance. These results indicate that both the density fluctuations and the IEFE have to be considered to comprehend the plasmas in high-density and density-fluctuating fluids.

DOI: 10.1103/PhysRevE.91.042316 PACS number(s): 61.05.fg, 51.50.+v, 52.80.−s, 77.22.Jp

I. INTRODUCTION

The particle number density (n) of fluids whose temperature (T) and pressure (P) are near the gas-liquid critical point (CP) fluctuates heavily, both spatially and temporally, on a microscopic scale [1–4]. Among the fluids near the CP, supercritical fluids (SCFs), which are fluids in a state where T and P are both above those at the CP, exhibit strong density fluctuations. As a consequence of the fluid structure being subjected to the density fluctuations, some physical and chemical properties of the fluids, such as the thermal conductivity [5–8] and the speed of sound [9], show anomalous behavior near the CP. In recent years, in addition to such critical anomalies of thermophysical properties, critical anomalies related to electrically charged particles have been reported, for example, local minima of breakdown voltages (U_B) in micrometer-scale discharges [10–14], local maxima of emission intensities in plasmas generated by pulsed laser ablation [15], and the peculiar behavior of cavitation bubbles subsequent to the generation of plasmas by pulsed laser ablation [16]. Moreover, increased yields in the syntheses of nanomaterials by discharge and laser-ablation plasmas in SCFs near the CP have been reported, such as silicon nanocrystals [17], nanodiamonds [18], and molecular diamond [19,20]. These critical anomalies imply that electron motion is highly affected by the local fluctuation of the particle density in fluids near the CP; however, studies on the motion of charged particles in such fluctuating fluids have not allowed us to clarify the mechanism of these critical anomalies.

In this study, we discuss the critical anomaly of U_B that has been observed in various fluids, such as carbon dioxide (CO_2) [10–12], water [12], xenon [12], air [13], and helium (He) [14]. In these studies, it was suggested that the local minima of U_B near the CP were caused by the concomitant effect of efficient electron acceleration in a void space and the low ionization potential of solid clusters [21–23], which are both generated by the density fluctuations [10,12]. To evaluate the effects of the density fluctuations on U_B, two models have been proposed. One was a modification of Paschen's law [24], which is a conventional empirical law where U_B is expressed as a similarity law as a function of the product of P and the gap distance (d), by combining it with a power law containing a dimensionless parameter F_D [10–12,14], which expresses the magnitude of the density fluctuations [1,2]. Although this modification allowed the reproduction of experimental U_B values in each fluid reasonably well, this model was purely phenomenological, making it difficult to link it to fundamental physical observations. The other approach was a model that introduced electron mean free paths near the CP, assuming a "hard-sphere cluster model" [14]. It was assumed in this model that the fluctuating fluids consist of spherical clusters and that the spaces between these clusters can be assimilated to form a particle-free region. However, since this model was too simple, it could only reproduce the presence of the critical anomaly of U_B near the CP and could not reproduce U_B quantitatively.

One of the notable characteristics of the critical anomaly of U_B is that it only has been observed in micrometer-scale discharges ($d < 5\,\mu$m) and that the local minimum of U_B was more pronounced for smaller d ($\sim$1−3 μm) [10,12]. For larger d ranging from 25 μm to 5 mm, the variation of U_B and the breakdown mechanisms in SCFs including the region near the CP have been studied [25–31]. However, these studies have not reported the existence of a local minimum of U_B near the CP, and the mechanism of the dependence of the critical anomaly of U_B on d has not yet been revealed.

A similar phenomenon, the deviation of U_B from Paschen's curve at atmospheric pressure, which has only been observed on the left branch of Paschen's curve in very small gap

*muneoka@plasma.k.u-tokyo.ac.jp
†kazuo@plasma.k.u-tokyo.ac.jp

discharges (typically: $d < 10\ \mu$m), has been investigated intensively [32–41]. The main motivation for these studies was the prevention of unintended breakdown leading to spark discharges as well as applications to gas sensing and analysis and lighting [33,41]. The values of U_B as a function of Pd, including the deviation from the conventional Paschen's law, form the so-called modified Paschen's curve [33–35]. Meanwhile, the deviation of U_B has also been observed for the right branch of Paschen's curve at very high P (typically: >1 MPa) [31,32,42–45]. The deviation from the right branch has been observed at larger d, for example, for $d = 1$ mm at about $P = 1000$ kPa at room temperature in air [44], for $d = 1.5$ mm at about $P = 80$ kPa at $T = 4.2$ K in He [31], and for $d = 10$ mm at about $P = 200$ kPa at room temperature in SF_6 [42]. The deviations from the conventional Paschen's curve have been reported to be caused by ion-enhanced field emission (IEFE) from the metal cathode [32], and those from the left branch of Paschen's curve can be reproduced by a mathematical formulation based on the Townsend breakdown model by modifying the secondary Townsend coefficient (γ) [33,38,39], which indicates the number of electrons emitted from the cathode per incident positive ion [46]. However, the validity of the numerical expression for the modified Paschen's curve has not yet been confirmed for high P.

For a more detailed investigation of the electrical breakdown in high-density fluids with strong density fluctuations, it is necessary to establish a new model of the electrical breakdown that reproduces two characteristics of the electrical breakdown near the CP, i.e., the critical anomaly itself and its dependence on d. In this paper, we propose an electrical breakdown model and discuss its validity by comparing U_B calculated using this model with the measured U_B. Moreover, we discuss the physics related to the electron motion in fluids with large density fluctuations. It is expected that this discharge model, which takes into account the density fluctuations, might provide further insights into the motion of charged particles in fluids exhibiting local density fluctuations, into the origin of the critical anomaly of the electrical breakdown, and into the other critical phenomena mentioned above.

II. ELECTRICAL BREAKDOWN MODEL CONSIDERING DENSITY FLUCTUATIONS

In general, an SCF has intermediate properties between a gas and a liquid, and can be divided into two regions by the so-called Widom line [47], which represents the local maxima of the density fluctuations F_D in the SCF state extending from the gas-liquid coexistence curve [3]: gaslike and liquidlike SCFs. Therefore, there are three approaches to discussing the properties and phenomena in an SCF: expanding existing theories from the gaseous phase (perhaps with some modifications), expanding those from the liquid phase (with modifications), or developing an original theory for SCFs. In this study, we adopted the first approach and we propose a model based on the conventional Townsend discharge model, in which the following equation is satisfied when breakdown occurs:

$$\gamma[\exp(\alpha d) - 1] \geqslant 1, \tag{1}$$

where α is the first Townsend coefficient, which indicates the number of ionization events caused by an electron in a unit-length path along an electric field. On this basis, we modified α due to the density fluctuations and γ due to the IEFE. We consider that the electrical discharges in the experiments in this study and in our previous study [14] were not corona- or streamerlike discharges because the gap distances were too short, the surfaces of the electrodes were too smooth, and the applied voltages were too small for such discharge modes to occur. In addition, while the breakdown voltages in liquid and liquidlike SCF regions were reported to be independent of the pressure in negative corona discharges [26,48], our experiments indicated the dependence of U_B on the pressure as shown in Sec. III. In the following, the effect of density fluctuations on α is discussed in Sec. II A, and then the modification of γ in the mathematical expression for the modified Paschen's curve is discussed in Sec. II B.

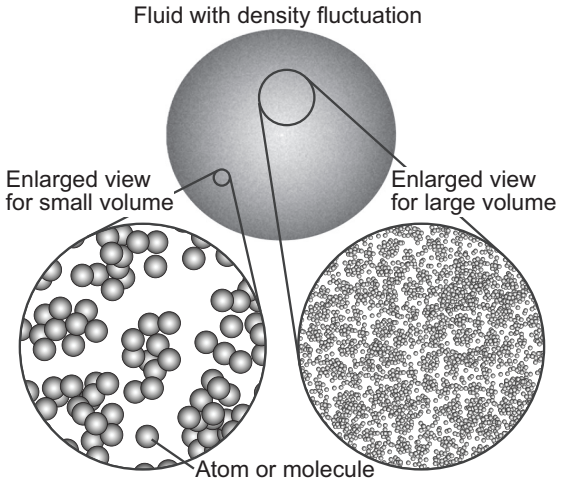

FIG. 1. Schematic of microscopic arrangements of fluid particles subjected to density fluctuations in domains with large and small volumes. The fluctuation of the local number density in a given volume is emphasized when the volume is small.

A. Modification of α due to density fluctuations

We introduce the effect of density fluctuations on electron motion in the space between electrodes and the consequent change in α. In our model, other significant effects of the density fluctuations are not included, such as the low ionization potential of cluster species, the generation of cluster ions, and the change in ion mobility due to clustering. In addition, the disturbance due to plasma-induced heating is not included because it can be assumed that the electrical breakdown occurs before the heating becomes dominant.

Figure 1 schematically illustrates the microscopic arrangements of fluid particles in domains with large and small volumes. The number of particles inside a given volume (indicated as a circle in the figure) heavily fluctuates spatially and temporally when the volume is comparable to the characteristic volume of the fluctuation. The main characteristic of our model is that it includes this nature of the density fluctuations. The relationship between the standard deviation (n_s) of the local number density (n_L) and the average number density (n_{ave}) can

be expressed using a nondimensional parameter F_D as [1]

$$\frac{n_s}{n_{ave}} = \sqrt{\frac{F_D}{n_{ave}V}}, \tag{2}$$

where

$$F_D \equiv \frac{\langle (N - \langle N \rangle)^2 \rangle}{\langle N \rangle} = \frac{(n_s V)^2}{n_{ave} V} = \frac{k_T}{k_T^0}, \tag{3}$$

where $\langle X \rangle$ indicates the average of X, N the number of molecules in a given volume V, k_T the isothermal compressibility, and k_T^0 the value of k_T for an ideal gas. Since k_T can be calculated from thermophysical databases, such as REFPROP [49], F_D can also be derived similarly to other thermophysical properties. Note that a larger F_D means larger density fluctuations and $F_D = 1$ in an ideal gas under any condition, which follows from the definition of F_D. Equation (2) indicates that n_s does not only depend on F_D and n_{ave} but also on V. In other words, n_s varies with V even under the same thermophysical conditions. This means that to discuss the effect of the density fluctuations on a specific phenomenon, we must evaluate the characteristic volume related to the phenomenon.

Our discharge model assumes that the electrical breakdown initiates in a locally low-density spatial domain caused by the density fluctuations. Figure 2 schematically illustrates the microscopic structure of fluid particles with a random distribution under conditions where the density fluctuations are negligible [Fig. 2(a)] and large [Fig. 2(b)]. An electron is accelerated by the applied electric field and collides with fluid particles inside the cylindrical volume along the electron path from the cathode to the anode. Figure 2 implies that an increase in F_D leads to an increase in the width of the distribution of the mean free path of the electron (λ) even at the same density and, as a result, λ can be larger in a local region of low density.

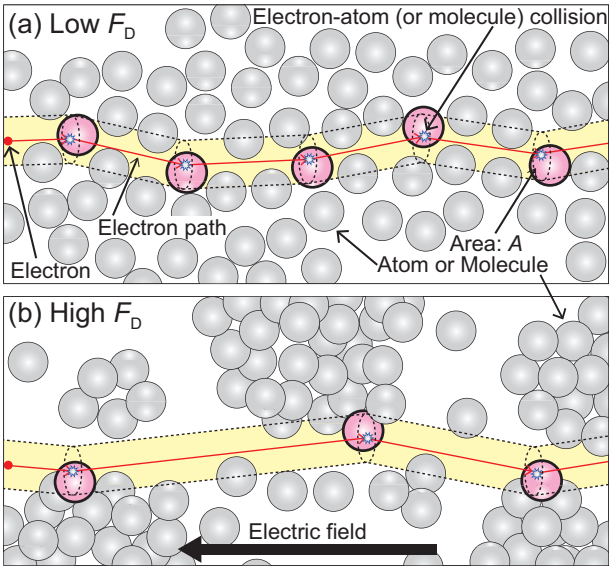

FIG. 2. (Color online) Schematic microscopic view of the cylindrical spatial domain along an electron path with a particle distribution and electron acceleration in (a) an ordinary gaseous fluid with low density fluctuations F_D and (b) a fluid with large density fluctuations (molecular clustering). An electron is accelerated by the applied electric field and collides with atoms or molecules whose centers are within the cylinder. The cross section of the cylinder is assumed to be the total collision cross section. The gray circles with thin circumferences indicate gas atoms or molecules and the circles with thick circumferences indicate atoms or molecules that collide with the electron.

On the basis of this assumption, we discuss α. We also assume that α/n can be expressed as a function of the reduced electric field (E/n), as is the case for a normal gas discharge. An expression for α/n can be obtained by solving the Boltzmann equation for an electron with employing cross-section databases or by the literature (for example, Ref. [46]) as an empirical expression (often using P instead of n, although P can only be used when the experimental conditions ensure proportionality between P and n):

$$\frac{\alpha}{n} = C_1 \exp\left[-C_2\left(\frac{E}{n}\right)^{-1}\right], \tag{4}$$

where C_1 and C_2 are constants. In the following, we discuss the effect of density fluctuations on the reduced electric field E/n.

Concerning E, a homogeneous electric field is assumed because there are only few charged particles between the electrodes before breakdown occurs and the geometry of the electrodes could be approximated as a plane-to-plane geometry as described in Sec. III A 1. Under this assumption, E is expressed as

$$E = \frac{U}{d}, \tag{5}$$

where U is the amplitude of the voltage between the electrodes. In the evaluation of n, the density of the local low-density spatial domain where the discharge occurs should be used in the estimation of α. Therefore, estimating the actual n_L where the discharge occurs is essential for calculating α. The effect of the density fluctuations on the value of n_L is discussed in the following.

Because of the density fluctuations, n_L at any given time and position has a distribution. Therefore, n_L can be expressed using n_{ave} and n_s as follows:

$$n_L = n_{ave} + x n_s = n_{ave}(1 + x n_s / n_{ave}), \tag{6}$$

where x is a parameter indicating the magnitude of the deviation from the average number density. The value of n_{ave} can be estimated from T and P using thermophysical databases such as REFPROP [49].

Figure 3 shows the distribution function of the local number density n under the assumption of a Gaussian distribution and the relationship between n_{ave}, n_s, n_L, and x. The value of x should be negative because n_L should be less than n_{ave} where breakdown occurs. In the present model, x is assumed to be constant for all conditions. This means that the proportion of the volume of the locally low-density spatial domain where breakdown can occur to the total volume between electrodes is constant, even if the conditions change. For example, if $x = -1$ when breakdown occurs and the distribution function of n_L is assumed to be Gaussian, then about 16% of the total volume must contribute to the electrical breakdown. Similarly,

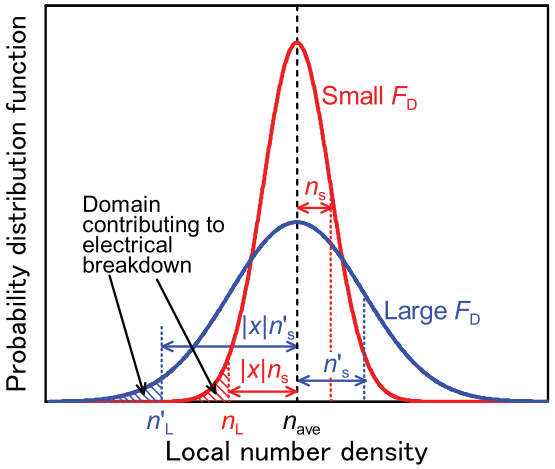

FIG. 3. (Color online) Schematic of the probability distribution function of the local number density with small and large density fluctuations F_D assuming that the probability distribution function is Gaussian. The relationships among the average number density n_{ave}, the standard deviation n_s (n'_s for a large F_D), the local number density in the cylindrical domain n_L (n'_L for a large F_D), and the parameter indicating the magnitude of the deviation from the average number density x is illustrated. For a large F_D, n'_L is lower than n_L at the same x. Domains with density lower than n_L (or n'_L) contribute to the electrical breakdown (shaded area). Note that the actual distribution of the local number density is not Gaussian and the skewness is not zero for almost all conditions.

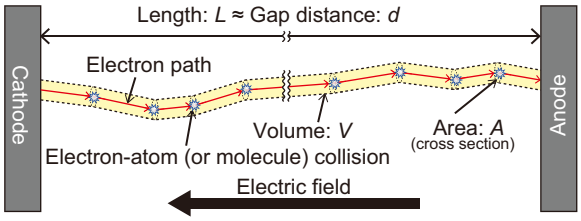

FIG. 4. (Color online) Schematic of cylindrical spatial domain along electron path between electrodes assumed in our model. As an electron travels from the cathode to the anode, it changes direction upon elastic and inelastic collisions with gas atoms or molecules in the high-density fluid (electron path). In our model, we assume that the length of the cylindrical spatial domain (yellow part along electron path) L is almost identical to the gap distance d.

if $x = -2$, then about 2.2% of the total volume must contribute to the initial breakdown. In the calculation, we treat x as a fitting parameter because we currently do not know how to obtain an analytical estimate of x. When F_D reaches a high level, i.e., at conditions near the CP, n_L is lower because n_s is higher and x is constant. Note that the skewness of the local number density distribution is not zero for a gas, liquid, or SCF, except for conditions corresponding to the Widom line [50]; in other words, the distribution is not symmetric with respect to the average number density for almost all conditions. Therefore, the above percentages are only approximate values.

As expressed by Eq. (2), n_s is related to both F_D and V. To evaluate V, we consider a local cylindrical spatial domain along the path of an electron that accelerates from the cathode to the anode (Fig. 4). Although the length of the cylinder (L) should exceed d because the direction of electron motion varies after each collision with a gas species, for simplicity, we assume that $L \approx d$. In high-pressure gases, since an electron does not gain sufficient energy for each collision to be inelastic, and because the electron is accelerated by repeated elastic collisions, the value of λ is important. When λ is small, the electron cannot easily gain sufficient energy between collisions. On the other hand, electrons can be accelerated efficiently for large λ. Therefore, to take into account collisions between all electron and gas species, including elastic and inelastic collisions, the cross section of the cylindrical spatial domain (A) is assumed to be the total collision cross section between the electron and gas species (σ). σ can be expressed as a function of the electron temperature (T_e). Under these assumptions, the volume of the cylinder (V) can be written as

$$V = AL = \sigma d. \tag{7}$$

From Eqs. (2) and (5)–(7), the effective reduced electric field in a locally low-density domain E/n_L can be expressed as

$$\frac{E}{n_L} = \frac{U/d}{n_{ave}[1 + x\sqrt{F_D/(n_{ave}\sigma d)}]}. \tag{8}$$

By determining the parameters related to the gas species (σ) and the experimental conditions (U, d, n_{ave}, and F_D) and by treating x as a fitting parameter, we can estimate the effective reduced field E/n_L. Then we can estimate α from E/n_L by solving Boltzmann's equation or Eq. (4). The values of the parameters used in this study are given in Sec. III A 2.

B. Modification of γ due to ion-enhanced field emission

To account for the effect of the high-density conditions on electrical discharges, the model includes the modification of γ due to IEFE. While the variation of the ion mobility (μ) depending on n is also included in our model (see Sec. III A 2), other major disturbances related to electrical discharges due to the high-density conditions and condensation, such as the change of collisional cross-sections due to clustering, are not included.

We briefly introduce the modification of γ in the mathematical formulation of the modified Paschen's curve [33,38,39]. Note that, although the mathematical formulation of the modified Paschen's curve introduced in this section is not our original model, this work is the first to apply it to the deviation of U_B in the right branch of Paschen's curve under high-pressure conditions.

IEFE is field emission enhanced by the thinning of the potential barrier in the vicinity of the cathode due to positive ions approaching the cathode [32,41]. The assumption in the mathematical formulation used in this study is that the potential field is linearly modified by the approaching ions. The effect of IEFE has recently been investigated by a fully analytical model of the distortion of an electric field by positive ions near the cathode [51]. However, the differences between the calculation results for U_B obtained by the model under the linear assumption and by the fully analytical model are small (<10%) [51]. Since the parameters in this study such as d have an uncertainty

of more than 10%, we consider that the model with the linear assumption is sufficiently accurate for this study.

The mathematical formulation of the modified Paschen's curve including the effect of IEFE is introduced by incorporating the potential field of the approaching ions into the Fowler-Nordheim equation. The Fowler-Nordheim equation gives the field emission current j_{FE} [52]:

$$j_{FE} = C_{FN} E_A^2 \exp\left(-\frac{D_{FN}}{E_A}\right), \tag{9}$$

where C_{FN} and D_{FN} are parameters related to the work function (ϕ) of the cathode and are loosely dependent on the electric field. The effective electric field on the cathode (E_A) is expressed as

$$E_A = \beta E, \tag{10}$$

where β is the geometric field-enhancement factor. Although field emission is known to be strongly affected by small protrusions on the surface, modeled by the factor β, and β can be estimated from the Fowler-Nordheim plot [53], we did not evaluate β in our experiments because of difficulties related to our experimental setup. The value of β has been reported to be at least 15 despite the use of carefully prepared surfaces [53] and, for example, a value of about 55 was used in investigations on the deviation of U_B from Paschen's curve in atmospheric-pressure micrometer discharges without considering the microscopic surface condition [38,39,54]. Therefore, in Sec. III, β is used as a fitting parameter in our calculation.

In the mathematical formulation of the modified Paschen's curve, γ is modified by IEFE as follows:

$$\gamma = \gamma_i + \gamma', \tag{11}$$

where γ_i is the secondary electron emission mainly due to the Auger neutralization effect [46] and γ' is that due to IEFE. The value of γ_i is assumed to be independent of P in this model. The following mathematical expression of γ' was originally suggested by Boyle and Kisliuk [32] and implemented by Radmilović-Radjenović and Radjenović [36]:

$$\gamma' = K \exp\left(-\frac{D_{FN}}{E_A}\right), \tag{12}$$

where K is a parameter, which has been analytically determined to be [39]

$$K = \frac{10 C_{FN} \beta^2 d}{\varepsilon_0 \mu}, \tag{13}$$

where ε_0 is the permittivity of vacuum.

C_{FN} and D_{FN} can be expressed as [55]

$$C_{FN} = a_1/[\phi t^2(y)], \tag{14a}$$

$$D_{FN} = a_2 \phi^{\frac{3}{2}} v(y), \tag{14b}$$

where $a_1 = 1.54 \times 10^{-6}$ A eV V^{-2}, $a_2 = 6.83 \times 10^9$ eV V m^{-1}, and $t(y)$ and $v(y)$ are nondimensional parameters that are functions of a nondimensional parameter y. y can be expressed as [55]

$$y = a_3 E_A^{1/2}/\phi, \tag{15}$$

where $a_3 = 3.79 \times 10^{-4}$ eV V$^{-1/2}$ m$^{-1/2}$. We estimated $v(y)$ [53,56] and $t(y)$ [53] to be

$$v(y) = 0.2792y^3 - 1.180y^2 - 0.09681y + 1, \tag{16a}$$

$$t(y) = -0.06394y^3 + 0.1422y^2 + 0.03176y + 1, \tag{16b}$$

which are expressions fitted to the values in the references. We confirmed that the differences between the values in the previous studies and the calculated values obtained from Eqs. (16a) and (16b) are within 3% for both $v(y)$ and $t(y)$.

From Eqs. (12)–(16), we can estimate γ' by determining the parameters E and d related to the experimental conditions. Finally, U_B can be estimated by substituting α calculated in Sec. II A and γ calculated in Sec. II B into Eq. (1).

III. EXPERIMENTAL AND NUMERICAL RESULTS

A. Experimental and calculation conditions

1. Experimental conditions

To evaluate the validity of the breakdown model explained above, we fitted the calculation results to experimental results for the measurement of U_B in He. The experimental setup and procedure for measuring U_B was identical to the one adopted in the previous study [14]. The critical temperature (T_c), critical pressure (P_c), and critical density (n_c) of He are 5.20 K, 227 kPa, and 17.4 mol L^{-1}, respectively. U_B was measured using tungsten (W) electrodes in a point-to-point configuration with tip radii of $25 \pm 5\,\mu$m and $d = 3 \pm 1\,\mu$m. We assume that the electric field between the electrodes was quasiuniform because the tip radii were sufficiently large in comparison with d. The adopted value of d in the calculation for fitting to the experimental results was 2.7 μm because the fitting curve was closest to the experimental results at $d = 2.7\,\mu$m. The temperature in the copper discharge cell was reduced by a 4 K Gifford-McMahon refrigerator system (RDK-205D and CKW-21, Sumitomo Heavy Industries), controlled by a temperature controller (Model 331, Lakeshore) by controlling the output current of a 50-W heater on the wall outside the chamber and fixed at 5.30 K ($T/T_c = 1.02$) or 5.50 K ($T/T_c = 1.06$). Experiments conducted using the same setup and the same method at 5.10 K ($T/T_c = 0.981$), 5.25 K ($T/T_c = 1.01$), and 5.40 K ($T/T_c = 1.04$) have been reported previously [14]. In this paper, we discuss the critical anomaly of U_B using the experimental data at $T = 5.25$, 5.30, and 5.50 K. The maxima of F_D at $T = 5.25$, 5.30, and 5.50 K are approximately 77, 40, and 14 at $P \sim 237$, 245, and 277 kPa, respectively, and these combinations of T and P are located on the Widom line. The pressure range was from 50 to 265 kPa at 5.30 K ($P/P_c = 0.22-1.17$) and from 50 to 300 kPa at 5.50 K ($P/P_c = 0.22-1.32$). These pressure ranges correspond to the range of n_{ave} from approximately 1 to 22 mol L^{-1}. We developed a measurement system to record T, P, and U_B simultaneously when electrical breakdown occurred. Since the measurements were conducted with a fixed inlet flow of 1 cm^3 min^{-1}, the pressure (density) continued increasing during the measurements and there should not be any duplicate measured U_B values at the same density. The increase in density between individual measurements was below 0.1 mol L^{-1}. However, in some figures in this paper,

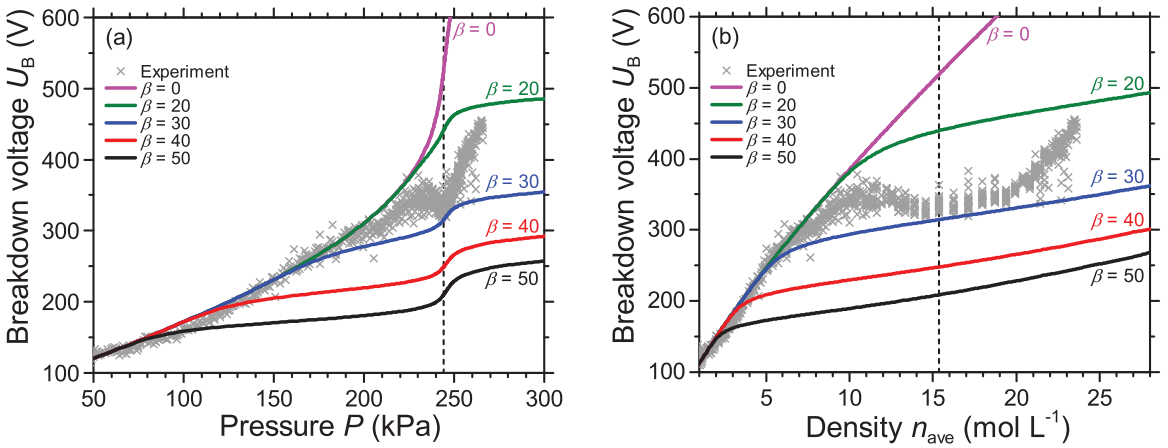

FIG. 5. (Color online) Variation of experimentally measured and numerically calculated U_B with β at $T = 5.30\,\mathrm{K}$ ($T/T_c = 1.02$) as a function of (a) pressure P and (b) density n_{ave} for He. A large β indicates a strong concentration of the electric field in the vicinity of protrusions on the cathode. The parameter x was set at -3 and the vertical dashed lines indicate the pressure or density on the Widom line at $T = 5.30\,\mathrm{K}$. The gap distance d was set at 2.7 μm. An ideal gas ($F_D = 1$) was assumed in the estimation of β without taking density fluctuations into account. The curve at $\beta = 0$ corresponds to the classical Paschen's curve.

some of the increases in density between measurements—especially near the CP—are larger than 0.1 mol L^{-1} and more than one value exists at the same density. This is because the isothermal compressibility was so high that we could not measure the difference in pressure for each measurement by our three-digit pressure gauge (PG35, Copal). To avoid any "conditioning effects" [31,44] that could affect the value of U_B, we started the measurements after more than 100 electrical discharges at each T. All values of n_{ave} in our experiments were calculated by REFPROP [49] using the measured values of T and P. Details of the discharge and measurement systems are given in Ref. [14].

2. *Calculation conditions*

To calculate U_B in our model, the properties (expressed by $\alpha, \phi, \gamma_i, \sigma$, and μ) should be determined. As mentioned in Sec. II A, α/n_L can be expressed as a function of E/n_L. This function was calculated by solving the Boltzmann equation using the Boltzmann equation solver BOLSIG+ [57] with a cross-section database of He [58] under the assumption that the difference in the ionization potentials between an isolated atom and its cluster is negligible because clusters in an SCF near the CP are very unstable [59]. In the He-W system, the work function ϕ and the secondary emission constant γ_i can be assumed to be 4.54 eV and 0.21, respectively [46]. We adopted the electron-atom impact (total) cross section of He [60] for σ, which is expressed as a function of the electron temperature (T_e). T_e was calculated as a function of E/n_L by BOLSIG+. Since the total cross section σ was only measured for T_e below 20 eV in the reference data [60], we conducted the calculation for values of T_e below 20 eV and all calculated data (shown in Figs. 5–11) satisfied $T_e < 20\,\mathrm{eV}$. Although the energy of electrons varies as they move along the path from the cathode to the anode, we did not take into account this temporal

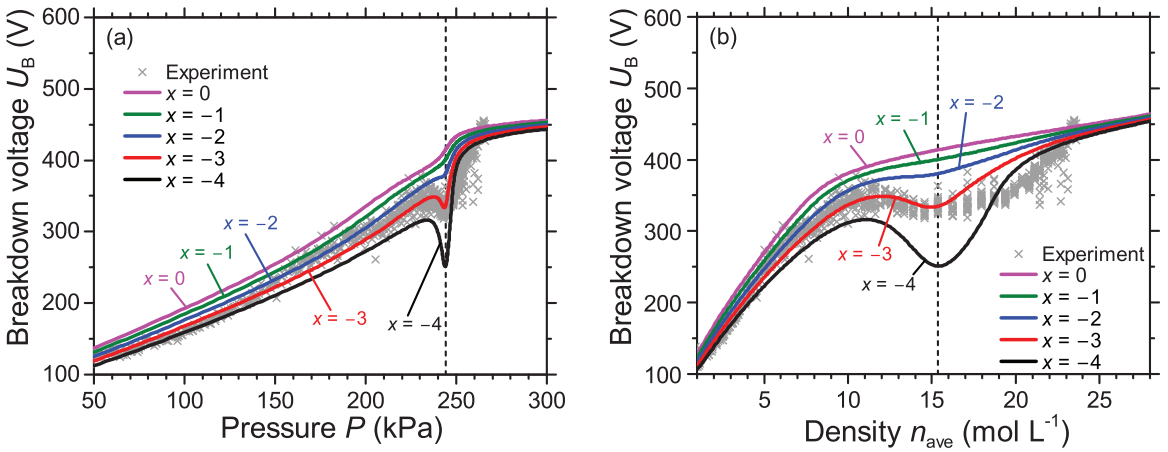

FIG. 6. (Color online) Variation of experimentally measured and numerically calculated U_B with different values of x at $T = 5.30\,\mathrm{K}$ ($T/T_c = 1.02$) in He as a function of (a) pressure P and (b) density n_{ave}. A small x (a large absolute value of x) indicates that the local volume n_L and the volume contributing to the initiation of electrical breakdown are small. β was set at 22 and the vertical dashed lines indicate the pressure or density on the Widom line at $T = 5.30\,\mathrm{K}$. The gap distance d was set at 2.7 μm. The experimental results are the same as those in Fig. 5.

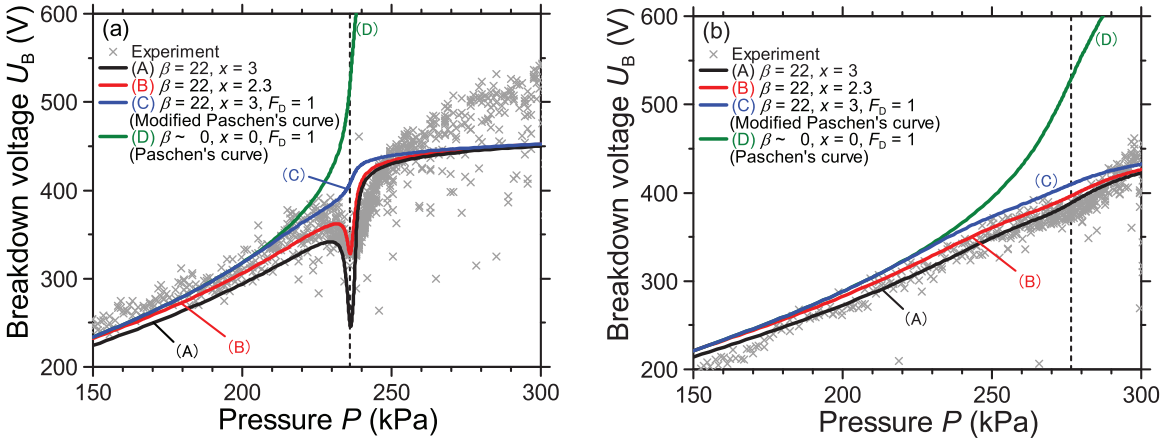

FIG. 7. (Color online) Experimentally measured and numerically calculated U_B as a function of P at (a) $T = 5.25\,\mathrm{K}$ ($T/T_c = 1.01$) and (b) $T = 5.50\,\mathrm{K}$ ($T/T_c = 1.06$) in He. The lines (A) and (B) indicate the results calculated by our model. The gap distance d was set at 2.7 μm. The line (C) is the modified Paschen's curve at $\beta = 22$ without taking into account the effect of the density fluctuations. The line (D) is the classical Paschen's curve. The vertical dashed lines indicate the pressures on the Widom line at $T = 5.25\,\mathrm{K}$ in (a) and 5.50 K in (b).

and spatial variation of energy and we used the average T_e value.

The ion mobility μ can be expressed using the reduced mobility μ_0 as

$$\mu = \mu_0 n_0 / n_L, \tag{17}$$

where n_0 is the number density of the gas at standard temperature ($T = 273.15\,\mathrm{K}$) and pressure ($P = 101.325\,\mathrm{kPa}$). The value of μ_0 was estimated using the effective reduced electric field E_A/n_L:

$$\mu_0 = 5.06 \times 10^{-3} \left(\frac{E_A}{n_L}\right)^{-0.4}, \tag{18}$$

which is the fitted expression of the values for He^+ in He at 5 K [61]. The units of μ_0 and E_A/n_L in Eq. (18) are $\mathrm{m^2\,V^{-1}\,s^{-1}}$ and Td ($=10^{-21}\,\mathrm{V\,m^2}$), respectively. Since the difference of μ_0 between 5 and 6 K at $E/n > 6\,\mathrm{Td}$ is sufficiently small (<2%) and the temperatures in our experiments were within this range, we used the values at 5 K in this paper. The error of μ_0 calculated by Eq. (18) relative to the values in Ref. [61] are within 1% for an electric field between 10 and 26 Td. All values of E/n_L in our calculation were >10 Td. Although there were no available data above 26 Td in Ref. [61], we used extrapolated values calculated by Eq. (18).

B. Comparison of model calculations with experiments in He

First, we evaluated the fitting parameter β by ignoring the effect of the density fluctuations. In the calculation, we set $F_D = 1$, which is the value for an ideal gas and similar to that for helium except near the critical point, and $x = -3$, which is the most appropriate value as will be discussed later. A large value of β indicates a large concentration of the

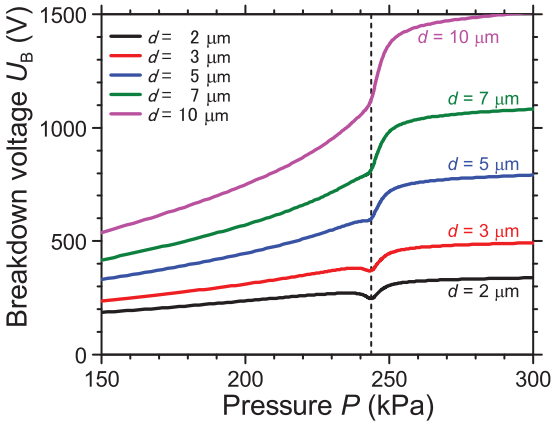

FIG. 8. (Color online) Calculated breakdown voltage U_B curves for different discharge gaps d as a function of He fluid pressure P. The temperature of the He fluid was fixed at 5.30 K and the fitting parameters β and x were 22 and -3, respectively, which were the best-fitted values in Figs. 5 and 6. The vertical dashed line indicates the pressure on the Widom line at $T = 5.30\,\mathrm{K}$. The local minimum of U_B near the pressure on the Widom line can be confirmed at $d \leqslant 5\,\mu\mathrm{m}$.

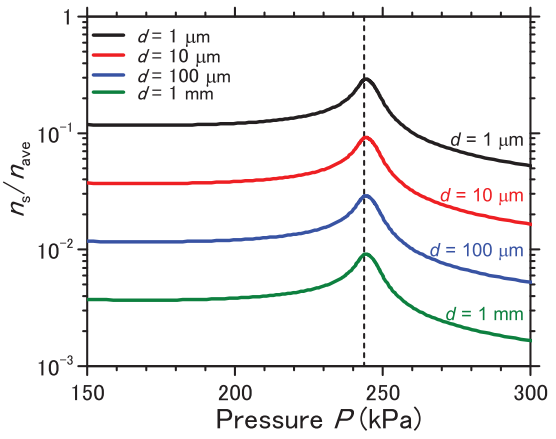

FIG. 9. (Color online) Ratio of the standard deviation n_s to the average number density n_{ave} for different gap distances d as a function of pressure P, calculated by Eq. (2). The temperature T, the cross section of a given volume A, and the parameter x were fixed at $T = 5.30\,\mathrm{K}$, $A = 5 \times 10^{-20}\,\mathrm{m^{-2}}$, and $x = -3$, respectively. Note that $x = -3$ was the best-fitted value in Fig. 6. The vertical dashed line indicates the pressure on the Widom line at $T = 5.30\,\mathrm{K}$.

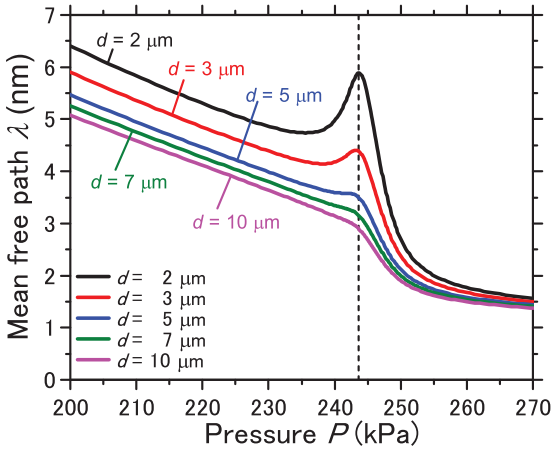

FIG. 10. (Color online) Calculated electron mean free path λ for different discharge gaps d as a function of He fluid pressure P when breakdown occurs. The temperature of the He fluid and the parameter x were fixed at 5.30 K and −3, respectively, where $x = -3$ was the best fitted value in Fig. 6. The local maximum of λ near the pressure on the Widom line can be confirmed at $d \leqslant 5\,\mu$m. The vertical dashed line indicates the pressure on the Widom line at $T = 5.30$ K.

electric field in the vicinity of protrusions on the cathode. The calculated U_B and the experimental results at 5.30 K are shown in Fig. 5 as functions of P [Fig. 5(a)] and n_{ave} [Fig. 5(b)]. The calculated and measured values of U_B in Figs. 5(a) and 5(b) were the same. For the horizontal axis, n_{ave} is a more important parameter than P for electric discharges in the gas phase (especially when the experimental conditions do not ensure proportionality between P and n), while the critical anomaly of U_B becomes more apparent when P is plotted on the x axis. Therefore, we show graphs plotted against both P and n_{ave} in the evaluation of the fitting parameters (Figs. 5 and 6). After that, we show the values of U_B and other parameters only as a function of P (Figs. 7–11). Figure 5 shows that the deviation of U_B from Paschen's curve starts at a lower pressure (density) at higher β and that β between 20 and 30 appears to be the most appropriate value for our experiments. This value is reasonable for IEFE as mentioned in Sec. II B. Actually, we adopted $\beta = 22$ because the most accurate calculation results were obtained with this value, as discussed in the following.

Next, the evaluation of the other fitting parameter x was conducted. The parameter F_D corresponding to the given thermophysical conditions was included in this calculation, with β set to 22. The calculation results at 5.30 K as functions of P and n_{ave} are shown in Figs. 6(a) and 6(b), respectively, where the indicated experimental results are the same as those in Fig. 5. Figure 6 shows that the U_B calculated by our model is in good agreement with the experimental results. The modification of U_B due to the density fluctuations was strongly emphasized near the pressure (density) on the Widom line and U_B has a local minimum when x is less than −2. As mentioned in the Introduction, since our electrical breakdown model is based on the electrical breakdown model for the gas phase, the breakdown model starts to deviate from the experimental results when the fluid state becomes a liquidlike SCF. The figure implies that $x \sim -3$ is the most appropriate value for this condition. A large absolute value of x indicates that the local volume n_L and the volume contributing to the initiation of the electrical breakdown are small. The value of −3 implies that the electron acceleration in 0.1% of the total volume, where the gas particle density is less than $n_{ave} - 3n_s$, contributes to the discharge ignition.

By comparing the results obtained at different temperatures, the dependence of the validity of our model on the thermophysical conditions can be discussed. Figure 7 shows the calculation results and experimental results at (a) 5.25 K ($T/T_c = 1.01$) and (b) 5.50 K ($T/T_c = 1.06$). The experimental results at 5.25 K are the values reported in Ref. [14], and those at 5.50 K were obtained in this study. The four lines shown in each graph in Fig. 7 are two fitting curves obtained by our model with $x = -3$ [line (A)] and −2.3 [line (B)], the modified Paschen's curve without the effect of the density fluctuations [line (C)] and the conventional Paschen's curve [line (D)]. The parameters for each line are indicated in the legends in Fig. 7. The calculation results in Fig. 7 reproduce the critical anomaly of U_B, in common with Fig. 6, and the critical anomaly is largest in the experimental results at 5.25 K, which is the value of T closest to T_c in this study. While Figs. 6 and 7(b) show

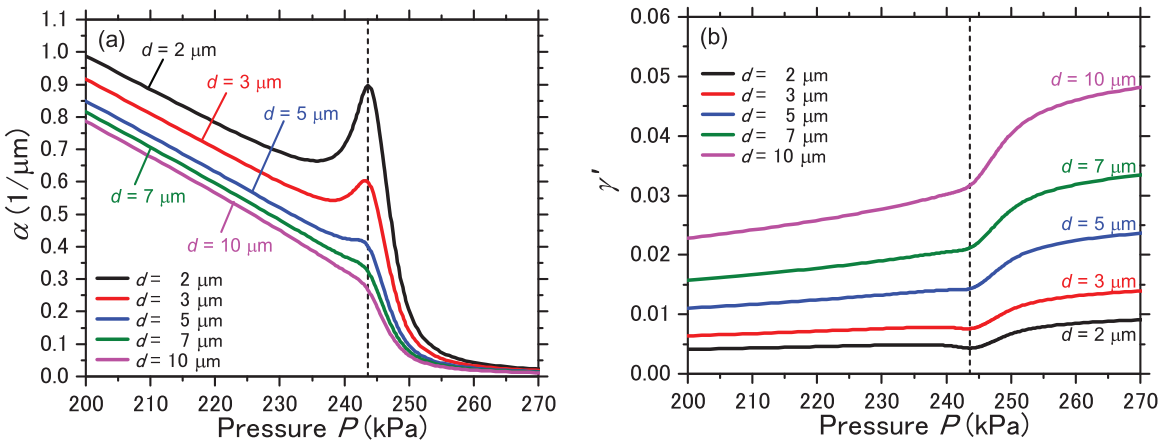

FIG. 11. (Color online) Calculated (a) first Townsend coefficient α and (b) secondary electron emission coefficient due to the IEFE γ', for different discharge gaps d as a function of He fluid pressure P at an electric field of $E = 125\,\mathrm{V}\,\mu\mathrm{m}^{-1}$, which was similar to the value of E when breakdown occurs. The temperature of the He fluid was fixed at 5.30 K and the parameters β and x are 22 and −3, respectively, which were the best-fitted values in Figs. 5 and 6. The vertical dashed lines indicate the pressure on the Widom line at $T = 5.30$ K.

that the fitting curve with $x = -3$ exhibits good agreement, in Fig. 7(a), the fitting curve with $x = -2.3$ has better agreement than that with $x = -3$. These results imply that the effect of the density fluctuations on U_B in our model is slightly overestimated or underestimated, although our breakdown model allows us to qualitatively simulate the U_B values well. It is expected that a more quantitative discussion will be possible once a more sophisticated analytical model that includes other clustering effects in high-density gases, such as the changes in ionization potential and ion mobility, has been proposed. An electrical breakdown model for the condensed phase that takes into account the density fluctuations will also be necessary for a more quantitative discussion.

C. Dependence of the effects of density fluctuations on the variation of U_B as a function of the gap distance

We also calculated U_B using the breakdown model to investigate the dependence of the critical anomaly on d. Figure 8 shows the calculation results of U_B for gap distances $d = 2, 3, 5, 7$, and 10 μm at a fixed temperature of 5.30 K. We did not calculate U_B for $d = 1$ μm because T_e exceeds 20 eV near the CP. As shown in the figure, the local minimum of U_B near the CP becomes evident with decreasing d, and the local decrease can be observed when d is less than approximately 5 μm. This result is in good agreement with the tendency of U_B measurements in high-density CO_2 near its CP with 1-, 5-, and 10-μm gap distances [12], and it is also consistent with the fact that no critical anomaly of U_B has been observed in studies with longer gap distances [25–31]. When d decreases, the volume of the locally low-density domain V at the breakdown decreases because of the smaller length L due to the assumption of $L \approx d$ in the breakdown model. As a result, n_s/n_{ave} increases when d decreases because n_s/n_{ave} is proportional to $V^{-0.5}$ [Eq. (2)]. In other words, as shown in Fig. 1, the effect of the density fluctuations on electron motion increases when V decreases. Our model has successfully included this nature of the density fluctuations, which is why the effect of the density fluctuations on U_B becomes significant with decreasing gap distance d.

As shown in Fig. 7(b), the calculated values of U_B [lines (A) and (B)] are smaller than those obtained by the modified Paschen's curve [line (C)], even for conditions relatively far from the critical point where the value of F_D is similar to that of an ideal gas (for example, $F_D < 2$). In other words, the effect of the density fluctuations on U_B emerges even under conditions far from the CP. This is due to the presence of the term xn_s/n_{ave} in Eq. (6). In contrast, the effect of the density fluctuations on U_B was not included in previous electrical breakdown models such as the conventional Townsend model [24] and the models for the modified Paschen's curve [33–35], although density fluctuations exist even in an ideal gas where $F_D = 1$. This is because in electrical discharges with macroscopic gap distances, the magnitude of n_s/n_{ave} and its change as a function of pressure are negligible. This is shown in Fig. 9, which displays the variation of n_s/n_{ave} for He as a function of pressure for gap distances between 1 μm and 1 mm, where the effect of the density fluctuations do not appear for gap distances larger than a few microns. Therefore, even if, in principle, the effect of the density fluctuations should be included in gaseous electrical breakdown models, it can be ignored for macroscopic gap distances.

IV. DISCUSSION OF THE EFFECTS OF DENSITY FLUCTUATIONS ON THE ELECTRON MEAN FREE PATH, α, AND γ

To discuss the electron motion in fluids using our model, we calculated the mean free path of an electron in a cylindrical spatial domain λ that can be expressed as follows:

$$\lambda = \frac{1}{n_L \sigma}. \tag{19}$$

Figure 10 shows the dependence of λ on d near the CP when breakdown occurs. The value of λ has a local maximum near the CP, which is due to the low n_L at high F_D, and this tendency corresponds to the concept shown in Fig. 2. Regarding the dependence of λ on d, both the value of λ and its increment near the CP are larger at smaller d. This is simply due to the dependence of n_L on d. Thus, the dependence of n_L on F_D is amplified with decreasing d.

In the following, the effects of the density fluctuations on the two coefficients α and γ in the discharge models are discussed. Figures 11(a) and 11(b) show the variation of the calculated values of α and γ' with different values of d as a function of P, respectively. The values in Fig. 11 are calculated for $T = 5.30$ K at a constant electric field of $E = 125$ V μm^{-1}, which is similar to the value of E when breakdown occurs near the CP in this study. As indicated in Fig. 11(a), the magnitude of α increases with decreasing d, and the value of α increases near the CP. Following Eq. (4), α can be expressed as the product of a linearly increasing component and a component that decreases exponentially with increasing n. Therefore, small values of n_L lead to large α. In other words, since electrons can easily be accelerated in the case of a large λ due to the large F_D, α is larger near the CP. Thus, the density fluctuations affect α by changing λ.

The value of γ' decreases with decreasing P, except for conditions near the CP and small values of d (<5 μm), as shown in Fig. 11(b). This can be explained as follows: since the IEFE is a probabilistic event, the long residence time of positive ions near the cathode due to high-P condition leads to an increase in the probability of IEFE. In other words, the decrease in the number density n due to decreasing P leads to a larger μ [Eqs. (17) and (18)], then the large μ causes a small K [Eq. (13)], and, finally, γ' decreases [Eq. (12)]. As shown in Figure 11(b), γ' increases with increasing d, and this is caused by the proportional relationships between γ' and K and between K and d [Eqs. (12) and (13)]. Figure 11(b) also indicates that γ' decreases slightly near the CP. This means that the effect of IEFE on U_B is suppressed when it is coupled to the density fluctuations, and U_B would increase by the variation of γ' near the CP if there would be no effect of the density fluctuations on α. The reason for this is proposed to be as follows. The decrease in the local number density n_L due to the density fluctuations leads to a higher μ, and the high μ causes a small γ', as derived from the same discussion as dependency of γ' on P (cf. the explanation further above). The magnitude of the decrease in γ' near the CP becomes smaller with increasing d, and this is also because

the effect of the density fluctuations is enhanced in small volumes.

Next, we discuss the relation between the density fluctuations and the IEFE near the CP, which both affect U_B. As mentioned above, while the variation of α near the CP in Fig. 11(a) tends to raise U_B, that of γ near the CP in Fig. 11(b) tends to drop U_B. However, the actual increase in U_B due to the decrease of γ' was not significant: The difference in U_B between the cases of considering and not considering the variation of γ' due to the density fluctuations was less than 0.5%. This is because the variation of γ' due to the density fluctuations was small and γ' is smaller than γ_i in this case. Moreover, as shown in Eq. (1), γ affects the Townsend criterion linearly, while α affects it exponentially. To summarize these points, a small n_L due to the density fluctuations leads to a larger α and smaller γ, but the variation of U_B near the CP is dominated by the effect of the variation of α due to the density fluctuations rather than γ.

V. CONCLUSION

We discussed two characteristics of electrical breakdown near the CP, i.e., the critical anomaly itself, evidenced by a local minimum and its dependence on d. We developed an electrical breakdown model based on an extension of the gas discharge theory (Townsend theory) with modifications of α due to the density fluctuations and γ due to the IEFE. For the modification of α, we developed a model based on the concept that the breakdown occurs in a locally low-density spatial domain resulting from the density fluctuations. The results of the model suggested that increasing F_D leads to an increase in the mean free electron path λ, leading to an increase of the first Townsend coefficient α in locally low-density spatial domains. Consequently, the enhanced electron acceleration causes the critical anomaly of U_B. Moreover, we reproduced the gap limitation of the critical anomaly of U_B by incorporating the nature of the density fluctuations in terms of their dependence on the characteristic volume in the model. Concerning the modification of γ due to IEFE, we confirmed that the mathematical expression for the modified Paschen's curve [33,38,39] can be used to derive the deviation of U_B from the right branch of the conventional Paschen's curve. We also found that, while the effect of IEFE is important for electrical discharges under high-pressure conditions, the modification of γ by the density fluctuations near the CP is negligible. These results and the discussion suggest that our breakdown model describes the microscopic relationship between electron acceleration and the density fluctuations well and therefore allows the microscopic density fluctuations to be linked to the macroscopic behavior of U_B. We believe that the discharge model presented in this work will not only improve studies on breakdown phenomena and electrical properties in high-pressure gases and SCFs including fluids near the CP but also allow the investigation of other critical anomalies that involve fluctuations, particularly in the field of electric discharges.

ACKNOWLEDGMENTS

This work was financially supported in part by a grant from the Ministry of Education, Culture, Sports, Science and Technology of Japan: a Grant-in-Aid for Scientific Research on Innovative Areas "Frontier Science of Interactions between Plasmas and Nano-interfaces" (Grant No. 21110002). This work was also supported in part by grants from the Japan Society for the Promotion of Science: a Grant-in-Aid for Scientific Research (B) (Grant No. 21360356), a Grant-in-Aid for Scientific Research (A) (Grant No. 24246120), and a Grant-in-Aid for JSPS Fellows (Grant No. 13J06697). The authors thank Dr. David Z. Pai of the University of Poitiers for helpful discussions on the field emission in high-density gases and SCFs.

[1] H. E. Stanley, *Introduction to Phase Transitions and Critical Phenomena* (Oxford University Press, Oxford, 1971).
[2] K. Nishikawa, K. Kusano, A. A. Arai, and T. Morita, J. Chem. Phys. **118**, 1341 (2003).
[3] K. Nishikawa and I. Tanaka, Chem. Phys. Lett. **244**, 149 (1995).
[4] K. Saitow, H. Ochiai, T. Kato, and K. Nishikawa, J. Chem. Phys. **116**, 4985 (2002).
[5] L. P. Kadanoff and J. Swift, Phys. Rev. **166**, 89 (1968).
[6] A. Tominaga, J. Low Temp. Phys. **16**, 571 (1974).
[7] A. Acton and K. Kellner, Phys. B+C **103**, 212 (1981).
[8] L. H. Cohen, M. L. Dingus, and H. Meyer, J. Low Temp. Phys. **49**, 545 (1982).
[9] J. V. Sengers and J. M. H. L. Sengers, Ann. Rev. Phys. Chem. **37**, 189 (1986).
[10] T. Ito and K. Terashima, Appl. Phys. Lett. **80**, 2854 (2002).
[11] T. Ito, H. Fujiwara, and K. Terashima, J. Appl. Phys. **94**, 5411 (2003).
[12] M. Sawada, T. Tomai, T. Ito, H. Fujiwara, and K. Terashima, J. Appl. Phys. **100**, 123304 (2006).
[13] D. A. Lacoste, H. Muneoka, D. Z. Pai, S. Stauss, and K. Terashima, Plasma Sources Sci. Technol. **21**, 052003 (2012).
[14] H. Muneoka, K. Urabe, S. Stauss, and K. Terashima, Appl. Phys. Express **6**, 086201 (2013).
[15] T. Kato, S. Stauss, S. Kato, K. Urabe, M. Baba, T. Suemoto, and K. Terashima, Appl. Phys. Lett. **101**, 224103 (2012).
[16] K. Urabe, T. Kato, S. Stauss, S. Himeno, S. Kato, H. Muneoka, M. Baba, T. Suemoto, and K. Terashima, J. Appl. Phys. **114**, 143303 (2013).
[17] K. Saitow and T. Yamamura, J. Phys. Chem. C **113**, 8465 (2009).
[18] H. Kikuchi, S. Stauss, S. Nakahara, F. Matsubara, T. Tomai, T. Sasaki, and K. Terashima, J. Supercrit. Fluids **55**, 325 (2010).
[19] S. Stauss, H. Miyazoe, T. Shizuno, K. Saito, T. Sasaki, and K. Terashima, Jpn. J. Appl. Phys. **49**, 070213 (2010).
[20] T. Shizuno, H. Miyazoe, K. Saito, S. Stauss, M. Suzuki, T. Sasaki, and K. Terashima, Jpn. J. Appl. Phys. **50**, 030207 (2011).
[21] C. Bréchignac, M. Broyer, Ph. Cahuzac, G. Delacretaz, P. Labastie, J. P. Wolf, and L. Wöste, Phys. Rev. Lett. **60**, 275 (1988).

[22] C. Y. Ng, in *Advances in Chemical Physics*, edited by I. Prigogine and Stuart A. Rice, Vol. 52 (John Wiley & Sons, New York, 1983).
[23] W. D. Knight, W. A. de Heer, and W. A. Saunders, Z. Phys. D Atoms, Mol. Clust. **3**, 109 (1986).
[24] F. Paschen, Ann. Phys. **273**, 69 (1889).
[25] J. Gerhold, IEEE Trans. Electr. Insul. **23**, 765 (1988).
[26] I. Ishii and T. Noguchi, Proc. Inst. Electr. Eng. **126**, 532 (1979).
[27] T. Furusato, T. Ihara, T. Kiyan, S. Katsuki, M. Hara, and H. Akiyama, IEEE Trans. Plasma Sci. **40**, 3105 (2012).
[28] T. Kiyan, A. Uemura, B. C. Roy, T. Namihira, M. Hara, M. Sasaki, M. Goto, and H. Akiyama, IEEE Trans. Plasma Sci. **35**, 656 (2007).
[29] T. Ihara, T. Furusato, S. Kameda, T. Kiyan, S. Katsuki, M. Hara, and H. Akiyama, J. Phys. D. Appl. Phys. **45**, 075204 (2012).
[30] K. Horii, M. Kosaki, A. J. Pearmain, and A. J. McNerney, Cryogenics (Guildf). **23**, 102 (1983).
[31] R. Meats, Proc. Inst. Electr. Eng. **119**, 760 (1972).
[32] W. S. Boyle and P. Kisliuk, Phys. Rev. **97**, 255 (1955).
[33] D. B. Go and D. A. Pohlman, J. Appl. Phys. **107**, 103303 (2010).
[34] R.-T. Lee, H.-H. Chung, and Y.-C. Chiou, IEE Proc. Sci. Meas. Technol. **148**, 8 (2001).
[35] A. Wallash and L. Levitb, Proc. SPIE **4980**, 87 (2003).
[36] M. Radmilović-Radjenović and B. Radjenović, IEEE Trans. Plasma Sci. **35**, 1223 (2007).
[37] M. Radmilović-Radjenović and B. Radjenović, Plasma Sources Sci. Technol. **17**, 024005 (2008).
[38] R. Tirumala and D. B. Go, Appl. Phys. Lett. **97**, 151502 (2010).
[39] P. Rumbach and D. B. Go, J. Appl. Phys. **112**, 103302 (2012).
[40] A. Venkattraman and A. A. Alexeenko, Phys. Plasmas **19**, 123515 (2012).
[41] D. B. Go and A. Venkattraman, J. Phys. D. Appl. Phys. **47**, 503001 (2014).
[42] A. H. Cookson, IEE Proc. A **128**, 303 (1981).
[43] A. H. Cookson, Proc. Inst. Electr. Eng. **117**, 269 (1970).
[44] D. Z. Pai, S. Stauss, and K. Terashima, Plasma Sources Sci. Technol. **23**, 025019 (2014).
[45] D. Z. Pai, S. Stauss, and K. Terashima, Plasma Sources Sci. Technol. **24**, 025021 (2015).
[46] Y. P. Raizer, *Gas Discharge Physics* (Springer-Verlag, Berlin, 1991).
[47] G. G. Simeoni, T. Bryk, F. A. Gorelli, M. Krisch, G. Ruocco, M. Santoro, and T. Scopigno, Nat. Phys. **6**, 503 (2010).
[48] S. Nakayama and D. Ito, Cryogenics (Guildf). **26**, 12 (1986).
[49] E. Lemmon, M. McLinden, and D. Friend, *NIST Standard Reference Database 23: Reference Fluid Thermodynamic and Transport Properties- REFPROP, Version 9.0* (National Institute of Standards and Technology, Standard Reference Data Program, Gaithersburg, 2012).
[50] T. Sato, M. Sugiyama, K. Itoh, K. Mori, T. Fukunaga, M. Misawa, T. Otomo, and S. Takata, Phys. Rev. E **78**, 051503 (2008).
[51] Y. Li and D. B. Go, J. Appl. Phys. **116**, 103306 (2014).
[52] R. H. Fowler and L. Nordheim, Proc. R. Soc. London. Ser. A, Contain. Pap. a Math. Phys. Character **119**, 173 (1928).
[53] R. Good and E. Müller, in *Encycl. Phys. vol. 21 Electron-Emission, Gas Disch. I* (Springer, Berlin, 1956), pp.176–231.
[54] Y. Li, R. Tirumala, P. Rumbach, and D. B. Go, IEEE Trans. Plasma Sci. **41**, 24 (2013).
[55] W. W. Dolan, Phys. Rev. **91**, 510 (1953).
[56] A. Burgess and H. P. Summers, Astrophys. J. **157**, 1007 (1969).
[57] G. J. M. Hagelaar and L. C. Pitchford, Plasma Sources Sci. Technol. **14**, 722 (2005).
[58] PHELPS database, [http://www.lxcat.net] (accessed 4 June 2013).
[59] C. C. Liew, H. Inomata, and S. Saito, Fluid Phase Equilib. **104**, 317 (1995).
[60] D. Andrick and A. Bitsch, J. Phys. B At. Mol. Phys. **8**, 393 (1975).
[61] A. S. Dickinson, M. S. Lee, and L. A. Viehland, J. Phys. B At. Mol. Opt. Phys. **32**, 4919 (1999).